Geophysical Research Letters

RESEARCH LETTER
10.1029/2023GL103595

Intensification of Mesoscale Convective Systems in the East Asian Rainband Over the Past Two Decades

Puxi Li[1], Fengfei Song[2,3], Haoming Chen[1], Jian Li[1], Andreas F. Prein[4], Wenxia Zhang[5], Tianjun Zhou[5], Moran Zhuang[6,7], Kalli Furtado[8], Mark Muetzelfeldt[9], Reinhard Schiemann[9], and Chao Li[10]

[1]State Key Laboratory of Severe Weather, Chinese Academy of Meteorological Sciences, China Meteorological Administration, Beijing, China, [2]Frontier Science Center for Deep Ocean Multispheres and Earth System and Physical Oceanography Laboratory, Ocean University of China, Qingdao, China, [3]Laoshan Laboratory, Qingdao, China, [4]National Center for Atmospheric Research, Boulder, CO, USA, [5]LASG, Institute of Atmospheric Physics, Chinese Academy of Sciences, Beijing, China, [6]CMA Earth System Modeling and Prediction Centre, China Meteorological Administration, Beijing, China, [7]Key Laboratory of Earth System Modeling and Prediction, China Meteorological Administration, Beijing, China, [8]Met Office, Exeter, UK, [9]National Centre for Atmospheric Science, Department of Meteorology, University of Reading, Reading, UK, [10]Max Planck Institute for Meteorology, Hamburg, Germany

Abstract As one of the major producers of extreme precipitation, mesoscale convective systems (MCSs) have received much attention. Recently, MCSs over several hotpots, including the Sahel and US Great Plains, have been found to intensify under global warming. However, relevant studies on the East Asian rainband, another MCS hotpot, are scarce. Here, by using a novel rain-cell tracking algorithm on a high spatiotemporal resolution satellite precipitation product, we show that both the frequency and intensity of MCSs over the East Asian rainband have increased by 21.8% and 9.8% respectively over the past two decades (2000–2021). The more frequent and intense MCSs contribute nearly three quarters to the total precipitation increase. The changes in MCSs are caused by more frequent favorable large-scale water vapor-rich environments that are likely to increase under global warming. The increased frequency and intensity of MCSs have profound impacts on the hydroclimate of East Asia, including producing extreme events such as severe flooding.

Plain Language Summary Mesoscale convective systems (MCSs), accounting for more than half of the total rainfall in the East Asian rainband, frequently generate high-impact extreme weather events, such as flooding. In the summer of 2020, large regions of East Asia suffered extensive flooding and damage. Therefore, understanding the long-term changes of MCSs is crucial to gain insights into how extreme weather may change in the context of global warming. However, compared to several other MCS hotpots, the investigation of long-term changes of MCSs is scarce over East Asia. Here, based on a high spatiotemporal resolution satellite precipitation product and a novel MCS tracking method, we find that MCSs have become more frequent and intense in the East Asian rainband and accounted for three quarters of the total rainfall increase during 2000–2021. It is further found that increases in atmospheric total column water vapor, which is mainly due to increased temperature caused by anthropogenic forcing, leads to more frequent large-scale water vapor-rich environments that are responsible for the intensification of MCSs. As water vapor increases with global warming, it is very likely that MCSs will continue to intensify in this region into the future.

Key Points:

- Mesoscale convective systems (MCSs) have become more frequent and intense in the East Asian rainband over the past two decades
- The significant increase of MCS precipitation accounted for three quarters of the total rainfall increase during 2000–2021
- The increase of atmospheric total column water vapor, mainly driven by anthropogenic forcing, leads to more favorable environments for MCSs

Supporting Information:

Supporting Information may be found in the online version of this article.

Correspondence to:

H. Chen and F. Song,
chenhm@cma.gov.cn;
songfengfei@ouc.edu.cn

Citation:

Li, P., Song, F., Chen, H., Li, J., Prein, A. F., Zhang, W., et al. (2023). Intensification of mesoscale convective systems in the East Asian rainband over the past two decades. *Geophysical Research Letters*, *50*, e2023GL103595. https://doi.org/10.1029/2023GL103595

Received 9 MAR 2023
Accepted 7 AUG 2023

Author Contributions:

Conceptualization: Puxi Li, Haoming Chen
Formal analysis: Puxi Li, Fengfei Song
Funding acquisition: Puxi Li, Haoming Chen
Investigation: Puxi Li, Fengfei Song, Haoming Chen, Jian Li, Andreas F. Prein, Wenxia Zhang, Moran Zhuang
Methodology: Puxi Li, Fengfei Song
Writing – original draft: Puxi Li, Fengfei Song, Haoming Chen

1. Introduction

Mesoscale convective systems (MCSs) are large, organized, deep, precipitating convective storms that extend hundreds of kilometers and last several hours or even more than 1 day (Feng et al., 2021; Houze, 2018; Schumacher & Rasmussen, 2020). They often occur in tropical regions and areas downstream of major mountain ranges, such as the Rocky Mountains, the Andes and the Himalayas (Feng et al., 2021; Kukulies et al., 2021; Schumacher & Rasmussen, 2020). As prolific rain-producers, they can contribute more than half of the total rainfall in these regions (Houze, 2018; Schumacher & Rasmussen, 2020). More importantly, they also tend to produce high-impact extreme weather events (e.g., flooding), due to their high intensity of precipitation, large sizes, and long duration (Houze, 2018). In the context of natural climate variability, it is important to investigate the long-term changes of MCSs to understand how extreme weather events may change under global warming (Donat et al., 2016; Prein et al., 2017b). This has not been possible until very recently, with the availability of

Writing – review & editing: Puxi Li, Fengfei Song, Haoming Chen, Jian Li, Andreas F. Prein, Wenxia Zhang, Tianjun Zhou, Moran Zhuang, Kalli Furtado, Mark Muetzelfeldt, Reinhard Schiemann, Chao Li

broadly deployed satellite observations (Feng et al., 2021) and ongoing developments in numerical modeling (Prein et al., 2015).

Progress has been made in analyzing the observed and projected changes of MCS under global warming in several MCS hotpots (Feng et al., 2016; Kahraman et al., 2021; Klein & Taylor, 2020; Prein et al., 2017a; Taylor et al., 2017). In the Sahel, it is reported that the frequency of extreme MCSs in the wet season has tripled during 1982–2016, which is attributed to the enhanced Saharan warming induced by the anthropogenic forcing (Fitzpatrick et al., 2020; Taylor et al., 2017). Over the U.S. Great Plains, intense and long-lived spring-time MCSs have occurred more frequently over the period of 1979–2014, which is related to the strengthened low-level jet (Feng et al., 2016, 2019). In addition to observational analysis, convection-permitting models have also been used to study the future changes of MCSs (Kahraman et al., 2021; Prein et al., 2017a). Over the U.S. Great Plains, the frequency of summertime intense MCSs is projected to increase by more than threefold by the end of 21st century under a high-emission scenario (Prein et al., 2017a). Over Europe, precipitation extremes and flood risks related to MCSs are also projected to increase (Kahraman et al., 2021). Over the Tibetan Plateau, Kukulies et al. (2021) identified and tracked MCSs in 2000–2019 and found that MCSs over the high mountains are generally smaller in size with shorter duration. However, over East Asia, another MCS hotpot (Fu et al., 2019; Yang et al., 2019; Zhang et al., 2018), downstream of the Tibetan Plateau and home to over 30% of the world's population, the investigation of the long-term changes of MCSs is relatively scarce compared to the above regions.

Here, by using a newly developed novel rain-cell tracking algorithm on a high spatiotemporal resolution satellite precipitation product, it is found that the frequency and intensity of MCSs have increased by 21.8% and 9.8% respectively during 2000–2021. The more frequent and intense MCSs contribute nearly three quarters of the total precipitation increase over this period. The changes in the MCSs are caused by more frequent favorable large-scale environments, a trend that will likely continue under a changing climate.

2. Methods

2.1. Observational, Reanalysis Datasets and Model Simulations Used

The Global Precipitation Measurement (GPM) Integrated Multi-satellitE Retrievals (IMERG) V06B precipitation product (Huffman et al., 2019; Tan et al., 2019) has been used to investigate the MCS changes over the East Asian rainband from 2000 to 2021. The GPM IMERG V06B precipitation product is an integrated retrieval data set from a network of GPM constellation satellite partners (Huffman et al., 2019), with a temporal resolution of 30 min and a spatial resolution of ∼10 km. Previous evaluation studies over the U.S. and China suggested that the MCS tracking results by using GPM IMERG precipitation product provides consistent results with those derived from ground-based radar data (Feng et al., 2021; Kukulies et al., 2021, 2023; Wu et al., 2023). It should be noted the hourly precipitation intensity could be changed due to the changes in the satellite constellation contributing to GPM IMERG, therefore, the efforts have been taken to ensure a seamless transition from TRMM to GPM (Huffman et al., 2019; Tan et al., 2019), and Tang et al. (2020) documented that there is little difference between the TRMM era (2013) and GPM era (2014–2015), which indicates that GPM IMERG is quite robust in the transition between the two eras. In addition, we have compared the trends of total precipitation in early summer among different precipitation products (details in Text S1 in Supporting Information S1). The results show that the increasing trends of total precipitation are evident among different precipitation products, and the GPM precipitation product has the stability to represent the trends of early-summer precipitation.

We also use the hourly high-resolution realization (around 31 km) integrated water vapor transport and its convergence, and total column water vapor (TCWV) derived from ERA5 reanalysis data set to reveal the large-scale environments associated with MCSs (Hersbach et al., 2020). The ERA5 is the fifth generation of the ECMWF atmospheric reanalysis of the global climate and was developed through the Copernicus Climate Change Service (C3S).

We use the monthly total column of water vapor output from 25 CMIP6 models (listed in Table S1 in Supporting Information S1) in historical simulations (from 2000 to 2014) and future projections (from 2015 to 2099) under SSP5-8.5 scenarios (Eyring et al., 2016; O'Neill et al., 2016). The first available realization for each model simulation is re-gridded to 1.0° × 1.0° (Lat × Lon) grid using first-order conservative interpolation, and then used to generate the multi-model ensemble mean (CMIP6 MME) using equal weight.

2.2. Tracking MCSs by Precipitation Features Over the East Asian Rainband

We use the hourly precipitation variable to identify and track MCSs, by applying an "iterative raincell tracking" (IRT) algorithm (Li et al., 2020; Moseley et al., 2019) based on the GPM IMERG precipitation product. Here an MCS is defined as an entity (persisting at least 2 hr) with precipitation ($\geq$3.0 mm hr^{-1}) covering an area exceeding 3,600 km^2, which aligns well with previous studies (Houze, 2018; Li et al., 2020; Schumacher & Rasmussen, 2020). For each MCS, the weighted rainfall center, rainfall area, hourly mean/max precipitation intensity within the area, duration, propagation speed and other precipitation characteristics are recorded (Moseley et al., 2019). More details on the IRT algorithm can be found in previous studies (Li et al., 2020; Moseley et al., 2019). It has been shown via additional sensitivity tests that, although the number of identified MCSs might change depending on the different threshold of rainfall intensity or area, the overall MCS features remain rather robust (Li et al., 2020). Therefore, different thresholds are unlikely to influence the primary results systematically revealed in this study.

2.3. Statistical Analysis

We track MCSs over East Asia (90.0°E–165.0°E; 2.5°N–50.0°N) in the early-summer season (June and July) during the period of 2000–2021, particularly focusing on the East Asian rainband (112.0°E–145.0°E; 25.0°N–37.0°N; blue boxes shown in Figure 1). An MCS is assigned to the East Asian rainband if its weighted rainfall center is located in this region in the first two hours of its lifetime. Another classification method based on the middle point of each MCS's entire track has also been performed, and this exhibits nearly the same results; thus our main findings are not sensitive to this choice.

To produce the MCS precipitation and total precipitation trends over East Asia during the past two decades in Figure 1, we calculate the linear trend and use two-tailed Student's *t*-tests to test the statistical significance level of the trends. Another non-parametric test and additional sensitivity tests on the potential impacts of 2020 on the trends of 2000–2021 have also been performed (Mondal et al., 2012; details in Text S2 in Supporting Information S1). The results show that the increasing precipitation trends remain robust under different significance tests, and the anomalous nature of 2020 is consistent with the long-term changes of MCSs in 2000–2021. In addition, following Groisman et al. (2005), the total MCS precipitation over the East Asian rainband has been sorted into different types according to various daily precipitation intensity (details in Table S2 in Supporting Information S1), to investigate each type's contribution to the increasing trend of total MCS precipitation.

For the linear trend analysis of accumulated amount induced by MCSs and composited precipitation averages over the East Asian rainband in Figure 3, we composite MCSs according to the location of the weighted rainfall center in each year, and calculated the accumulated precipitation of all MCSs and the average precipitation in every individual MCS at each grid point, within 100.0 km from the MCS weighted rainfall center. Then we calculate the linear trend and the statistical significance level with two-tailed Student's *t*-tests.

To provide a more visible and intuitive description of the changes of MCS features, we not only calculate linear trends of MCS features in terms of the changes per decade, but also give the increasing percentage of total changes across the entire period (2000–2021) relative to the climatology (the average between 2000 and 2021).

2.4. Selection of Similar Circulation Patterns at MCS Initiation

We use TCWV to further investigate the changes of similar large-scale environments favorable for MCS initiation (details in Text S3 in Supporting Information S1), a similar method has been used to investigate the past and future changes of large-scale environments favorable for MCS over the U.S. Great Plains (Song et al., 2022).

3. Results

3.1. Spatial Distributions and Linear Trends of MCS Precipitation

In the early-summer season, East Asia is largely influenced by the East Asian summer monsoon system (Ding & Chan, 2005; Xie & Sampe, 2010) which forms a Meiyu (China)-Baiu (Japan)-Changma (Korean) rainband along ~30°N (Figure 1a). In this period, successive MCSs form, propagate eastward along this rainband and often generate persistent extreme precipitation and floods in active years (Cheng et al., 2022; Guan et al., 2020).

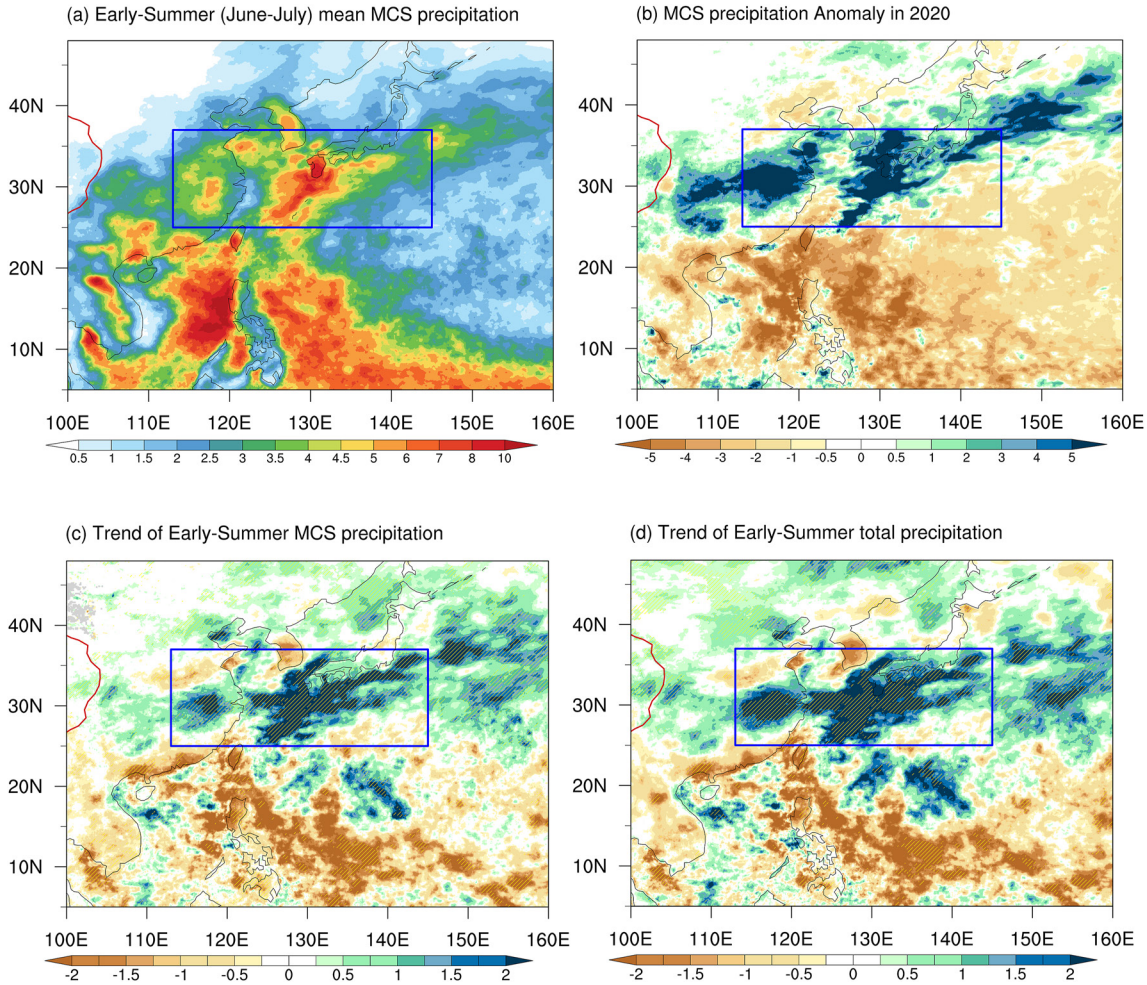

Figure 1. Mesoscale convective systems (MCSs) contributed the majority of the increasing trend of total precipitation in early summer over East Asia during the past two decades (from 2000 to 2021). (a) Early-summer MCS precipitation climatology (unit: mm day^{-1}). (b) Early-summer MCS precipitation anomalies in 2020 (unit: mm day^{-1}). (c) The MCS precipitation trend during the past two decades (unit: mm day^{-1} decade^{-1}). (d) The same as (c), but for the total precipitation trend. Grid points with a statistical significance exceeding the 95% confidence level (with a two-tailed Student's *t*-test) are marked by yellow diagonal lines. The red contour indicates the Tibetan Plateau (the topography exceeds 2,700 m). The blue boxes indicate the target domain (the East Asian rainband), where the statistical analyses have been performed.

For example, in 2020, large regions of East Asia experienced an exceptionally wet rainy season (Figure S1b in Supporting Information S1) and intense MCS precipitation (Figure 1b), which led to severe impacts and consequential economic losses (Clark et al., 2021). In the Yangtze River Valley, 2020 was the wettest summer since 1998 (Ding et al., 2021; Volonté et al., 2021), but no significant El Niño event was observed, which is widely considered as a dominant factor at the inter-annual timescale (Liu et al., 2020; Volonté et al., 2021). Hence, it is important to see whether the MCSs over East Asia have changed in the past and whether the anomaly in 2020 may reflect part of the long-term change. The anomaly of early-summer MCS precipitation in 2020 (Figure 1b) agrees well with the changes of the MCS precipitation and total precipitation from 2000 to 2021 (Figures 1c and 1d), with pattern correlation coefficients of 0.63 and 0.58, respectively. The East Asian rainband has experienced a statistically significant increase of MCS precipitation, with rates exceeding 2.0 mm day^{-1} per decade (Figure 1c), which accounts for most of the total precipitation changes (Figure 1d).

We examine the time series of MCS precipitation, as well as the daily means of MCS precipitation within each early summer over the East Asian rainband (Figure 2). The total precipitation exhibits an increasing trend at a linear rate of 1.16 mm day^{-1} per decade, with large inter-annual variability (Figure 2a). The wetting trend of total precipitation is primarily due to the increase in MCS precipitation, which shows a linear trend of 0.87 mm day^{-1} per decade (i.e., increased by 54.5% over 2000–2021), accounting for three quarters of the increase in the total

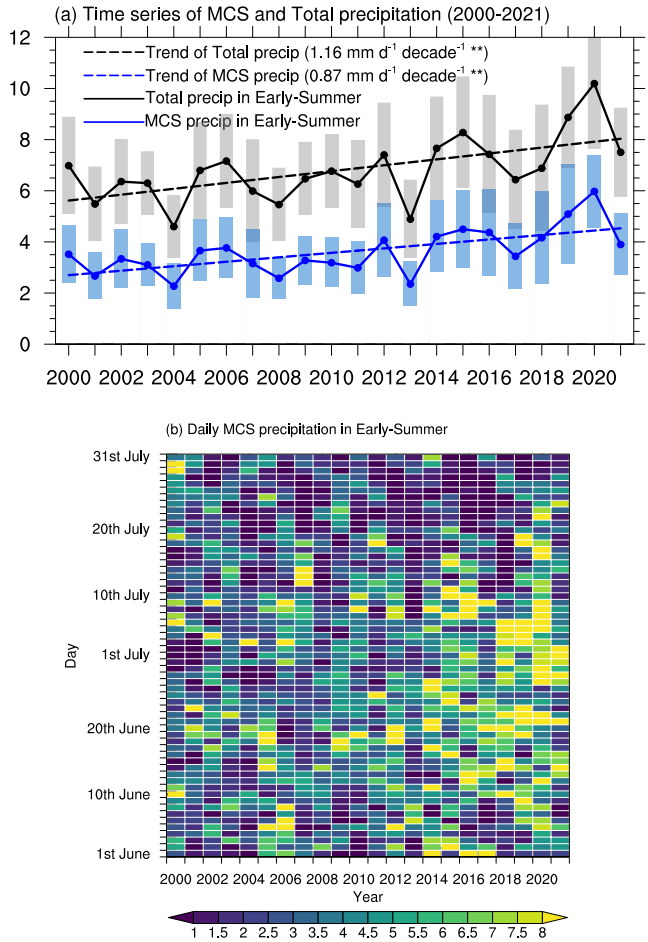

Figure 2. Time series and linear trends of MCS and total precipitation, and daily mean MCS precipitation within each early-summer season over the East Asian rainband. (a) Time series of early-summer MCS (blue) and total (black) precipitation (unit: mm day^{-1}), and linear trends of MCS (blue dashed line) and total precipitation (black dashed line; both statistically significant at 99% with two-tailed Student's *t*-tests) of early summer (unit: mm day^{-1} decade^{-1}). Here the gray/blue shadings represent the ±0.5 standard deviations of the daily total/MCS precipitation in each early-summer. (b) Daily mean MCS precipitation (unit: mm day^{-1}) within each early-summer season during the past two decades (2000–2021).

rainfall (Figure 2b). After sorting the total MCS into different types according to the daily precipitation accumulation, it is shown that all three types of MCS precipitation exhibit significant increasing trends in 2000–2021 (Table S2 in Supporting Information S1). The extreme MCS precipitation (daily accumulation exceeds 100.0 mm) has the highest increasing rate of 0.39 mm d^{-1} decade^{-1} and has a contribution of 44.8% to the increasing trend of total MCS. In addition, there is an increase in the variance of daily MCS precipitation averaged over the East Asian rainband (Figure 2a), and more days over the East Asian rainband have experienced intense MCS precipitation (≥5mm day^{-1}; Figure 2b). For example, generally, there are 9.9 days over East Asian rainband experiencing intense MCS precipitation during the first decade (2000–2010), but this has almost doubled to 18.9 days in the recent decade (2011–2021). Hence, intense MCS precipitating days are becoming more frequent, as was the case in 2020. As a result, the contribution from MCSs to total precipitation over the East Asia rainband region has increased from 50.1% in the first decade to 55.3% in the second decade (Figure S2 in Supporting Information S1).

3.2. Linear Trends of MCS Precipitation Characteristics

To reveal the detailed changes of MCS precipitation over the East Asia rainband, we investigated changes of hourly MCS precipitation frequency-intensity structures. The probability density function of MCS precipitation shows that moderate to heavy hourly precipitation (5.0∼100.0 mm hr^{-1}) became more frequent in the past two decades (Figure 3a). This is consistent with an increase of intense MCS precipitation days (Figure 2b). The intensity changes are also evident in both the hourly average and maximum precipitation intensity, with rates of 0.31 mm hr^{-1} decade^{-1} (increased by 9.8% over 2000–2021) and 3.3 mm hr^{-1} decade^{-1} (∼24.4%), respectively (Figures S3b and S3c in Supporting Information S1). Moreover, short-lived (+39.8 decade^{-1}) MCSs and long-lived (+34.7 decade^{-1}) MCSs (Figure S3a in Supporting Information S1) contribute almost equally to the increasing trend of total MCSs (+74.6 decade^{-1}; i.e., increased by 21.8% in the past two decades from 2000 to 2021).

We further investigate the linear trends of the composited accumulated precipitation induced by all MCSs (Figure 3b) and the precipitation averaged within each individual MCS (Figure 3c), through a Lagrangian perspective analysis following the location of MCS precipitation centers. A notable increase is seen in the accumulated rainfall amount produced by all MCSs (according to the MCS precipitation center), with the trend of rainfall near the MCS center exceeding 700.0 mm decade^{-1} (Figure 3b). In addition, each MCS generally produces more rainfall, with hourly precipitation intensity showing a significant upward trend, at a rate of 0.5 mm hr^{-1} decade^{-1} on average (Figure 3c). No significant changes are seen in the MCS rainfall area (Figure S3d in Supporting Information S1) and MCS duration (not shown).

This means that more frequent MCSs have occurred over the same area with higher intensity in the past two decades. This much larger accumulated rainfall can cause severe flooding, as was seen in the 2020 rainy season. To summarize, MCSs have become more frequent and intense in the past two decades, which dominates the increased MCS precipitation over the East Asia rainband, without significant changes in rainfall area or duration.

3.3. The Changes of the Associated Large-Scale Atmospheric Circulations

To investigate the potential drivers of MCS changes over the East Asian rainband, composite analysis of the large-scale environments at MCS initiation is conducted. A similar method has also been used in previous studies

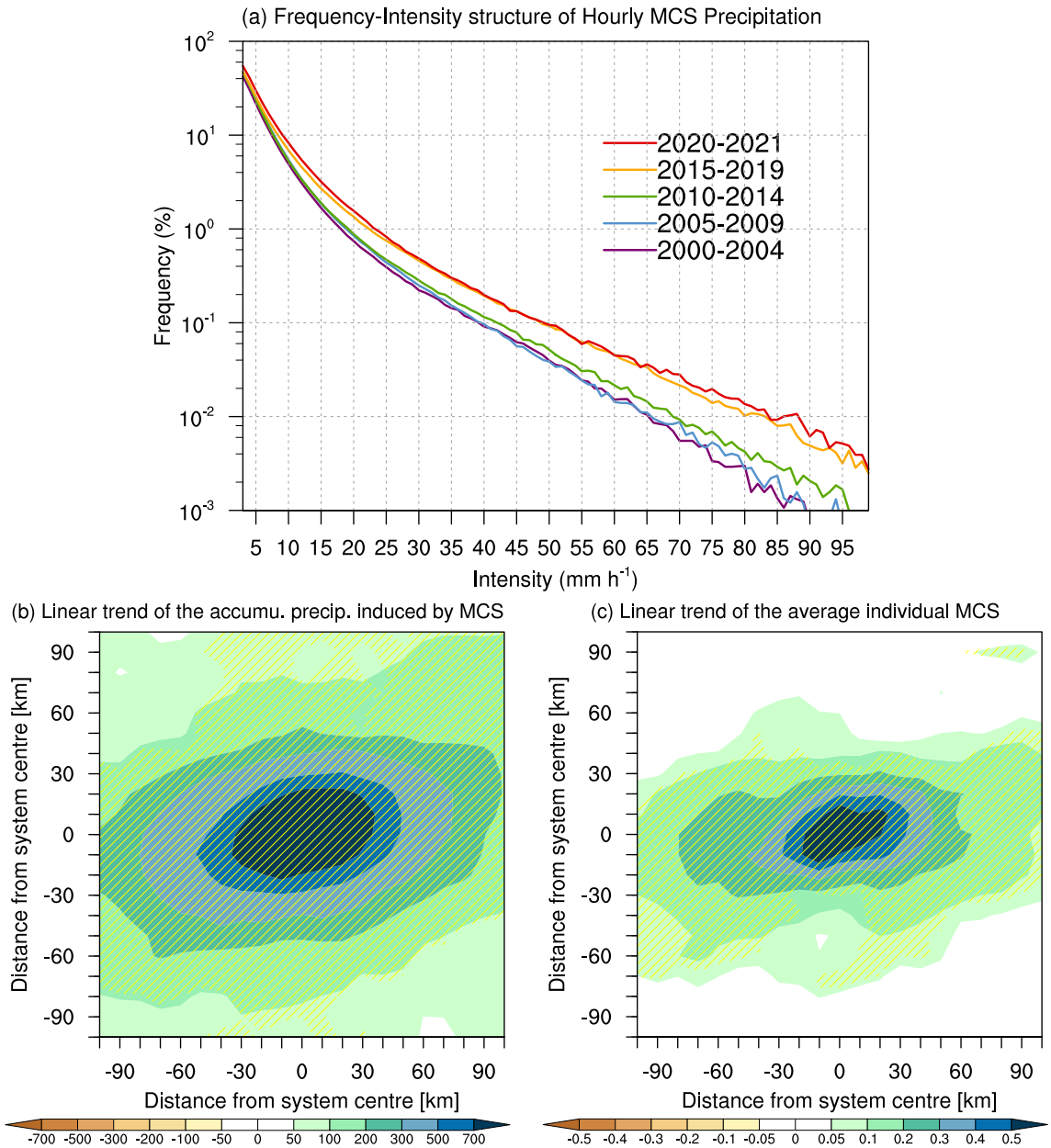

Figure 3. Probability density function of MCS hourly precipitation, and linear trends of the accumulated amount and the composited precipitation averages according to the location of the MCS precipitation center. (a) Frequency-Intensity structure of MCS hourly precipitation over the East Asian rainband. Linear trends of the (b) composited accumulated rainfall amount (unit: mm decade^{-1}) produced by all MCS and (c) hourly precipitation averages of each individual MCS (unit: mm h^{-1} decade^{-1}) in each early-summer season from 2000 to 2021. Grid points with a statistical significance exceeding the 95% confidence level are marked by yellow diagonal lines, with two-tailed Student's *t*-tests.

(Kukulies et al., 2021; Yang et al., 2017). We only select MCS initiation moment of the MCS to minimize the feedback impact of MCSs on the large-scale environment. The composited anomalies of integrated water vapor transport and its convergence when MCSs initiate are shown in Figure 4a. The strong integrated water vapor transport is evident over the western flank of the Western North Pacific Subtropical High at MCS initiation (Figure 4a), which brings abundant moisture from the tropical ocean to the East Asian rainband. In addition, there is also another northerly/northeasterly branch of water vapor transport from higher latitudes (Figure 4a). As a result, the convergence/divergence of the integrated water vapor transport shows a triple pattern (Figure 4a): a strong and narrow band of zonal convergence over the East Asian rainband region with two divergence regions to the north and south respectively. This moisture convergence zone provides moist instability favorable for the

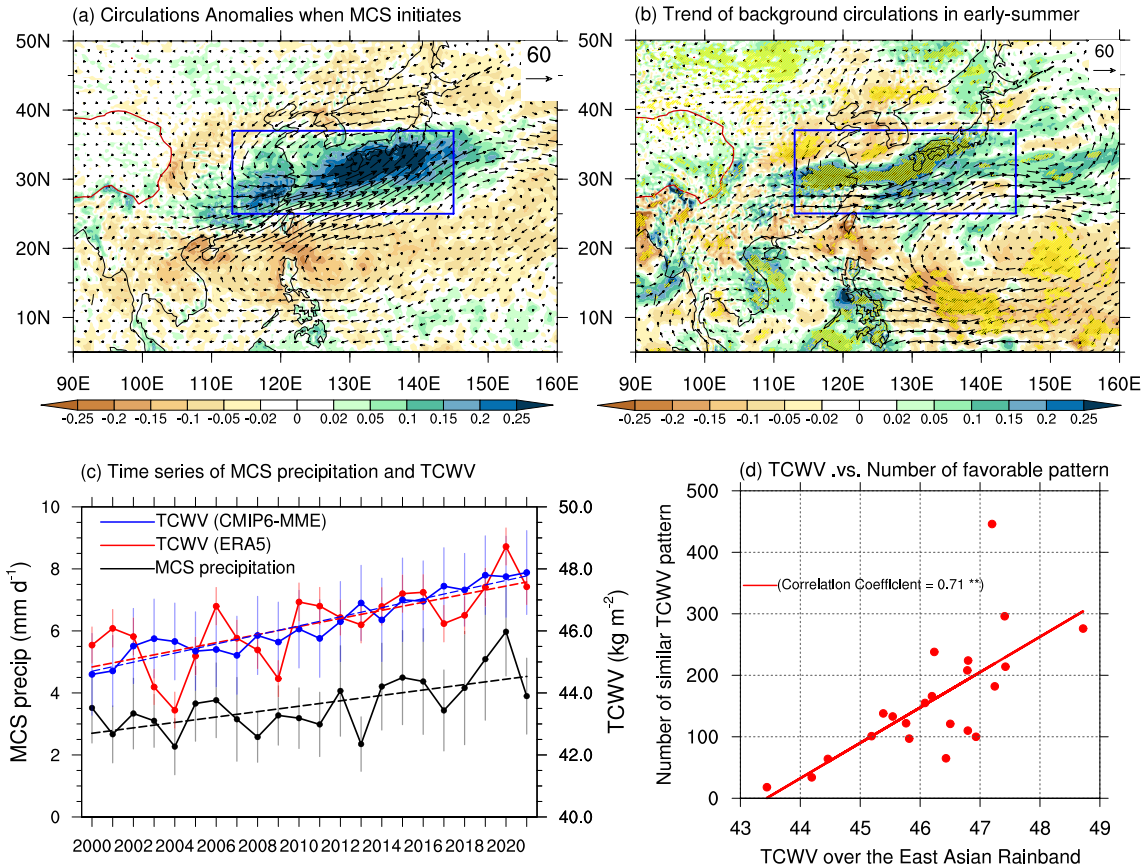

Figure 4. Large-scale environment anomalies when MCSs initiate over the East Asian rainband and changes of atmospheric circulations in the early-summer season during the last two decades. (a) The composited circulation anomalies when MCSs initiate compared to the early-summer climatology. The integrated water vapor transport and its convergence are indicated by the vectors (unit: kg m^{-1} s^{-1}) and shadings (unit: 10^{-4} kg m^{-2} s^{-1}), respectively. (b) The linear trends of the early-summer mean integrated water vapor transport (unit: kg m^{-1} s^{-1} $decade^{-1}$) and its convergence (unit: 10^{-4} kg m^{-2} s^{-1} $decade^{-1}$). Grid points with a statistical significance exceeding the 95% confidence level (with two-tailed Student's *t*-tests) are marked by yellow diagonal lines. The red contour indicates the Tibetan Plateau (the topography exceeds 2700 m). (c) Time series and linear trends of TCWV (unit: kg m^{-2}) in ERA5 reanalysis (red) and CMIP6 multi-model ensemble mean (MME; blue), and MCS precipitation (unit: mm day^{-1}; black) over the East Asian rainband (indicated by the blue box). The linear trends of TCWV and MCS precipitation are all statistically significant at 99% with two-tailed Student's *t*-tests. Here the gray/red bars represent the ±0.5 standard deviation of the daily precipitation/TCWV in each early summer. The blue bars indicate the ±0.5 standard deviation of the 25 CMIP6 models to represent the inter-model spread. (d) The relationship between the early-summer mean TCWV over the East Asian rainband (unit: kg m^{-2}) and the number of similar hourly TCWV patterns in each year during 2000–2021.

enhancement of deep convection and the formation of MCSs (Figure 4a). The anomalies of the large-scale environments, observed 3 hr prior to MCS initiation, generally display a similar pattern in the integrated water vapor transport and its convergence, but exhibit a smaller magnitude compared to those observed at MCS initiation (Figure S4a in Supporting Information S1). The anomalies when no MCS initiates are opposite to those observed at the initiation moment (Figure S4b in Supporting Information S1 and Figure 4a): specifically, the integrated water vapor transport over the western flank of the Western North Pacific Subtropical High is weaker compared to the climatology, and the moisture convergence zone has also weakened over the target region. These contrasts in the large-scale anomalies between the MCS-initiating and the non-MCS-initiating situations highlight the unique environments that are capable of supporting MCS initiation. In addition, the linear trends of atmospheric circulations in the entire early-summer season over the past two decades are evident in Figure 4b. The phenomenon of note is that the integrated water vapor transport by the southwesterly circulations surrounding the Western North Pacific Subtropical High has been enhanced, as well as the northerlies in higher latitudes. Therefore, the East Asian rainband experienced a significant increase in convergence of integrated water vapor transport (Figure 4b).

The variation of water vapor transport convergence can be understood as two main terms, one related to the varied wind convergence and the other is related to the varied TCWV. When MCSs initiate, the water vapor transport convergence anomaly is closely related to the TCWV anomaly (Figure 4a vs. Figure S5a in Supporting

Information S1), with a high pattern correlation coefficient of 0.63. Further, TCWV and MCS precipitation also have a close relationship (Figure 4c), with a correlation coefficient of 0.73, significant at the 99% confidence level. Thus, TCWV can be used to represent the changes of water vapor transport convergence.

The trends of integrated water vapor transport and its convergence are consistent with the anomalies when MCSs initiate over the East Asian rainband (Figure 4b vs. Figure 4a), indicating that the large-scale background environments have become more favorable for MCS formation. To further confirm this, we use TCWV patterns to determine and investigate the changes of similar large-scale environments favorable for MCS initiation (see Methods). The favorable TCWV pattern resembles the one with MCS initiation (Figure S5b in Supporting Information S1), and becomes more intense and frequent over the past two decades (Figure S5c and S5d in Supporting Information S1). As a result, TCWV in early summer generally becomes more favorable for the formation of more frequent and intense MCSs over the East Asian rainband (Figure S5e in Supporting Information S1). The more frequent and intense favorable TCWV pattern is closely related to the increased water vapor in the recent two decades (Figure S5f in Supporting Information S1), and the correlation coefficient of the two annual time series between the TCWV and the MCS precipitation over the East Asian rainband is 0.71 (Figure 4d). This means that more water vapor favors more favorable MCS initiation environments, leading to more MCSs. From the CMIP6 models, the increased water vapor during 2000–2021 is mainly contributed by global warming (Figure 4c). Progressing global warming increases TCWV due to its dependence on air temperature following the Clausius-Clapeyron relationship (Held & Soden, 2006), so TCWV is projected to increase further in the 21st century following a high-emission scenario (Figure S6 in Supporting Information S1). Previous studies also suggest the East Asian summer monsoon circulation may also be enhanced under global warming (Kamae et al., 2014; Li et al., 2019, 2022). Hence, we may expect more frequent and intense MCSs in the East Asian rainband in the future.

4. Summary

A narrow latitudinal rainband in the early summer season is a prominent feature of East Asian meteorology. MCSs contribute more than half of the total rainfall amount in this rainband. In the past two decades (2000–2021), we found that large areas of the East Asian rainband have experienced a statistically significant increase of precipitation that is mostly driven by MCS rainfall, with rates locally exceeding 2.0 mm day^{-1} per decade. MCS precipitation over the East Asian rainband region shows a linear trend of 0.87 mm day^{-1} per decade (i.e., increased by 54.5% over 2000–2021), accounting for three quarters of the increase in total rainfall. The contribution from MCSs to total rainfall has also significantly increased. In addition, the intense MCS precipitating days (≥5.0 mm day^{-1}) have become more frequent, with 9.9 days on average from 2000 to 2010, rising to 18.9 days from 2011 to 2021.

From 2000 to 2021, the East Asian rainband region experienced more intense MCSs, which caused a significant increase in MCS precipitation. The more frequent MCSs over East Asian rainband (+74.6 decade^{-1}; increased by 21.8% in the past two decades) with almost equal contributions from both long-lived (+34.7 decade^{-1}) and short-lived (+39.8 decade^{-1}) MCSs. In addition, both the hourly average and maximum precipitation intensity have also experienced significant increase, with rates of 0.31 mm hr^{-1} decade^{-1} and 3.3 mm hr^{-1} decade^{-1}, respectively. Thus, MCSs have become more frequent and intense, contributing significantly to the total rainfall changes in East Asia.

The trends of early-summer integrated water vapor transport and its convergence highly resemble those of MCS initiation, indicating that the large-scale background environment has become more favorable for MCS formation. Further analysis shows that the increased water vapor convergence is closely related to the TCWV, which is correlated to MCS precipitation. In the previous two decades, water vapor-rich environments have become more frequent, which is favorable for forming more frequent and intense MCSs over the East Asian rainband. The increased column water vapor in the East Asian rainband during 2000–2021 is mainly caused by the anthropogenic forcing, which will be further amplified in the future.

In this study, we discovered that MCSs over the East Asian rainband have exhibited a notable increase in both frequency and intensity over the past two decades. The increase in column atmospheric water vapor has contributed to a higher occurrence of environments conducive to MCS initiation, but it is important to note that long-term projections of MCS occurrence and intensity could be influenced by additional feedbacks and processes that have not been addressed here. The relative contributions of changes in the thermodynamic (i.e., water

vapor) and dynamical (i.e., wind convergence) environments to the MCS changes, and the regional differences in the changes of MCS features between land and oceanic regions need to be further investigated by conducting convection-permitting model simulations in the future.

Conflict of Interest

The authors declare no conflicts of interest relevant to this study.

Data Availability Statement

The GPM IMERG V06B precipitation product is available at https://gpm.nasa.gov/data/directory. The GPCP precipitation product is available at https://www.ncei.noaa.gov/data/global-precipitation-climatology-project-gpcp-daily/access/. The CMORPH precipitation product is available at https://www.ncei.noaa.gov/data/cmorph-high-resolution-global-precipitation-estimates/access/30min/8km/. The ERA5 reanalysis data set is available at http://climate.copernicus.eu/products/climate-reanalysis. CMIP6 model simulations (listed in Table S1 in Supporting Information S1) are from the Earth System Grid Federation (https://esgf-node.llnl.gov/search/cmip6/). The code used to generate the figures and table are based on NCAR Command Language (NCL v6.6.2; http://www.ncl.ucar.edu/). The IRT program codes used to identify and track mesoscale convective systems are publicly available in https://github.com/christophermoseley/iterative_raincell_tracking.

Acknowledgments
This research is jointly supported by the National Natural Science Foundation of China (U2142214, 42005039, and 42105026) and the National Key R&D Program of China (2021YFC3000904). This is a contribution no 16 to CORDEX-FPS-CPTP. The authors acknowledge the NASA for making GPM V06B precipitation product publicly available. The authors also acknowledge the World Climate Research Programme's Working Group on Coupled Modeling and the climate modelling groups (listed in Table S1 in Supporting Information S1) for producing and making available the CMIP6 model simulations. The authors also thank the Copernicus Climate Change Service (C3S) for providing the ERA5 reanalysis data set publicly.

References

Cheng, T. F., Dong, Q., Dai, L., & Lu, M. (2022). A dual regime of mesoscale convective systems in the East Asian monsoon annual cycle. *Journal of Geophysical Research: Atmospheres*, *127*(13), e2022JD036523. https://doi.org/10.1029/2022jd036523

Clark, R. T., Dong, X., Ho, C.-H., Sun, J., Yuan, H., & Takemi, T. (2021). Preface to the special issue on summer 2020: Record rainfall in Asia—Mechanisms, predictability and impacts. *Advances in Atmospheric Sciences*, *38*(12), 1977–1979. https://doi.org/10.1007/s00376-021-1010-5

Ding, Y., & Chan, J. C. L. (2005). The East Asian summer monsoon: An overview. *Meteorology and Atmospheric Physics*, *89*(1–4), 117–142. https://doi.org/10.1007/s00703-005-0125-z

Ding, Y., Liu, Y., & Hu, Z. Z. (2021). The record-breaking Mei-Yu in 2020 and associated atmospheric circulation and tropical SST anomalies. *Advances in Atmospheric Sciences*, *38*(12), 1980–1993. https://doi.org/10.1007/s00376-021-0361-2

Donat, M. G., Lowry, A. L., Alexander, L. V., O'Gorman, P. A., & Maher, N. (2016). More extreme precipitation in the world's dry and wet regions. *Nature Climate Change*, *6*(5), 508–513. https://doi.org/10.1038/nclimate2941

Eyring, V., Bony, S., Meehl, G. A., Senior, C. A., Stevens, B., Stouffer, R. J., & Taylor, K. E. (2016). Overview of the coupled model intercomparison project phase 6 (CMIP6) experimental design and organization. *Geoscientific Model Development*, *9*(5), 1937–1958. https://doi.org/10.5194/gmd-9-1937-2016

Feng, Z., Houze, R. A., Leung, L. R., Song, F., Hardin, J. C., Wang, J., et al. (2019). Spatiotemporal characteristics and large-scale environments of mesoscale convective systems east of the Rocky Mountains. *Journal of Climate*, *32*(21), 7303–7328. https://doi.org/10.1175/jcli-d-19-0137.1

Feng, Z., Leung, L. R., Hagos, S., Houze, R. A., Burleyson, C. D., & Balaguru, K. (2016). More frequent intense and long-lived storms dominate the springtime trend in central US rainfall. *Nature Communications*, *7*(1), 13429. https://doi.org/10.1038/ncomms13429

Feng, Z., Leung, L. R., Liu, N., Wang, J., Houze, R. A., Li, J., et al. (2021). A global high-resolution mesoscale convective system database using satellite-derived cloud tops, surface precipitation, and tracking. *Journal of Geophysical Research: Atmospheres*, *126*(8), e2020JD034202. https://doi.org/10.1029/2020jd034202

Fitzpatrick, R. G., Parker, D. J., Marsham, J. H., Rowell, D. P., Guichard, F. M., Taylor, C. M., et al. (2020). What drives the intensification of mesoscale convective systems over the West African Sahel under climate change? *Journal of Climate*, *33*(8), 3151–3172. https://doi.org/10.1175/jcli-d-19-0380.1

Fu, S.-M., Mai, Z., Sun, J.-H., Li, W.-L., Ding, Y., & Wang, Y.-Q. (2019). Impacts of convective activity over the Tibetan Plateau on plateau vortex, southwest vortex, and downstream precipitation. *Journal of the Atmospheric Sciences*, *76*(12), 3803–3830. https://doi.org/10.1175/jas-d-18-0331.1

Groisman, P. Y., Knight, R. W., Easterling, D. R., Karl, T. R., Hegerl, G. C., & Razuvaev, V. N. (2005). Trends in intense precipitation in the climate record. *Journal of Climate*, *18*(9), 1326–1350. https://doi.org/10.1175/jcli3339.1

Guan, P., Chen, G., Zeng, W., & Liu, Q. (2020). Corridors of Meiyu-season rainfall over Eastern China. *Journal of Climate*, *33*(7), 2603–2626. https://doi.org/10.1175/jcli-d-19-0649.1

Held, I. M., & Soden, B. J. (2006). Robust responses of the hydrological cycle to global warming. *Journal of Climate*, *19*(21), 5686–5699. https://doi.org/10.1175/jcli3990.1

Hersbach, H., Bell, B., Berrisford, P., Hirahara, S., Horányi, A., Muñoz-Sabater, J., et al. (2020). The ERA5 global reanalysis. *Quarterly Journal of the Royal Meteorological Society*, *146*(730), 1999–2049. https://doi.org/10.1002/qj.3803

Houze, R. A. (2018). 100 years of research on mesoscale convective systems. *Meteorological Monographs*, *59*, 17.11–17.54. https://doi.org/10.1175/amsmonographs-d-18-0001.1

Huffman, G. J., Stocker, E. F., Bolvin, D. T., Nelkin, E. J., & Tan, J. (2019). *GPM IMERG final precipitation L3 half hourly 0.1 degree x 0.1 degree V06*. Goddard Earth Sciences Data and Information Services Center (GES DISC). https://doi.org/10.5067/GPM/IMERG/3B-HH/06

Kahraman, A., Kendon, E. J., Chan, S. C., & Fowler, H. J. (2021). Quasi-stationary intense rainstorms spread across Europe under climate change. *Geophysical Research Letters*, *48*(13), e2020GL092361. https://doi.org/10.1029/2020gl092361

Kamae, Y., Watanabe, M., Kimoto, M., & Shiogama, H. (2014). Summertime land–sea thermal contrast and atmospheric circulation over East Asia in a warming climate—Part I: Past changes and future projections. *Climate Dynamics*, *43*(9–10), 2553–2568. https://doi.org/10.1007/s00382-014-2073-0

Klein, C., & Taylor, C. M. (2020). Dry soils can intensify mesoscale convective systems. *Proceedings of the National Academy of Sciences of the United States of America*, *117*(35), 21132–21137. https://doi.org/10.1073/pnas.2007998117

Kukulies, J., Chen, D., & Curio, J. (2021). The role of mesoscale convective systems in precipitation in the Tibetan Plateau region. *Journal of Geophysical Research: Atmospheres*, *126*(23), e2021JD035279. https://doi.org/10.1029/2021jd035279

Kukulies, J., Lai, H. W., Curio, J., Feng, Z., Lin, C., Li, P., et al. (2023). Mesoscale convective systems in the third pole region: Characteristics, mechanisms and impact on precipitation. *Frontiers in Earth Science*, *11*, 1143380. https://doi.org/10.3389/feart.2023.1143380

Li, P., Moseley, C., Prein, A. F., Chen, H., Li, J., Furtado, K., & Zhou, T. (2020). Mesoscale convective system precipitation characteristics over East Asia. Part I: Regional differences and seasonal variations. *Journal of Climate*, *33*(21), 9271–9286. https://doi.org/10.1175/jcli-d-20-0072.1

Li, T., Wang, Y., Wang, B., Ting, M., Ding, Y., Sun, Y., et al. (2022). Distinctive South and East Asian monsoon circulation responses to global warming. *Science Bulletin*, *67*(7), 762–770. https://doi.org/10.1016/j.scib.2021.12.001

Li, Z., Sun, Y., Li, T., Ding, Y., & Hu, T. (2019). Future changes in East Asian summer monsoon circulation and precipitation under 1.5 to 5 C of warming. *Earth's Future*, *7*(12), 1391–1406. https://doi.org/10.1029/2019ef001276

Liu, B., Yan, Y., Zhu, C., Ma, S., & Li, J. (2020). Record-breaking Meiyu rainfall around the Yangtze River in 2020 regulated by the subseasonal phase transition of the North Atlantic Oscillation. *Geophysical Research Letters*, *47*(22), e2020GL090342. https://doi.org/10.1029/2020gl090342

Mondal, A., Kundu, S., & Mukhopadhyay, A. (2012). Rainfall trend analysis by Mann-Kendall test: A case study of north-eastern part of Cuttack district, Orissa. *International Journal of Geology, Earth and Environmental Sciences*, *2*(1), 70–78.

Moseley, C., Henneberg, O., & Haerter, J. O. (2019). A statistical model for isolated convective precipitation events. *Journal of Advances in Modeling Earth Systems*, *11*(1), 360–375. https://doi.org/10.1029/2018ms001383

O'Neill, B. C., Tebaldi, C., Van Vuuren, D. P., Eyring, V., Friedlingstein, P., Hurtt, G., et al. (2016). The scenario model intercomparison project (ScenarioMIP) for CMIP6. *Geoscientific Model Development*, *9*(9), 3461–3482. https://doi.org/10.5194/gmd-9-3461-2016

Prein, A. F., Langhans, W., Fosser, G., Ferrone, A., Ban, N., Goergen, K., et al. (2015). A review on regional convection-permitting climate modeling: Demonstrations, prospects, and challenges. *Reviews of Geophysics*, *53*(2), 323–361. https://doi.org/10.1002/2014RG000475

Prein, A. F., Liu, C., Ikeda, K., Trier, S. B., Rasmussen, R. M., Holland, G. J., & Clark, M. P. (2017a). Increased rainfall volume from future convective storms in the US. *Nature Climate Change*, *7*(12), 880–884. https://doi.org/10.1038/s41558-017-0007-7

Prein, A. F., Rasmussen, R. M., Ikeda, K., Liu, C., Clark, M. P., & Holland, G. J. (2017b). The future intensification of hourly precipitation extremes. *Nature Climate Change*, *7*(1), 48–52. https://doi.org/10.1038/nclimate3168

Schumacher, R. S., & Rasmussen, K. L. (2020). The formation, character and changing nature of mesoscale convective systems. *Nature Reviews Earth & Environment*, *1*(6), 300–314. https://doi.org/10.1038/s43017-020-0057-7

Song, F., Leung, L. R., Feng, Z., Chen, X., & Yang, Q. (2022). Observed and projected changes of large-scale environments conducive to spring MCS initiation over the US Great Plains. *Geophysical Research Letters*, *49*(15), e2022GL098799. https://doi.org/10.1029/2022gl098799

Tan, J., Huffman, G. J., Bolvin, D. T., & Nelkin, E. J. (2019). IMERG V06: Changes to the morphing algorithm. *Journal of Atmospheric and Oceanic Technology*, *36*(12), 2471–2482. https://doi.org/10.1175/jtech-d-19-0114.1

Tang, G., Clark, M. P., Papalexiou, S. M., Ma, Z., & Hong, Y. (2020). Have satellite precipitation products improved over last two decades? A comprehensive comparison of GPM IMERG with nine satellite and reanalysis datasets. *Remote Sensing of Environment*, *240*, 111697. https://doi.org/10.1016/j.rse.2020.111697

Taylor, C. M., Belusic, D., Guichard, F., Parker, D. J., Vischel, T., Bock, O., et al. (2017). Frequency of extreme Sahelian storms tripled since 1982 in satellite observations. *Nature*, *544*(7651), 475–478. https://doi.org/10.1038/nature22069

Volonté, A., Muetzelfeldt, M., Schiemann, R., Turner, A. G., & Klingaman, N. (2021). Magnitude, scale, and dynamics of the 2020 Mei-Yu rains and floods over China. *Advances in Atmospheric Sciences*, *38*(12), 2082–2096. https://doi.org/10.1007/s00376-021-1085-z

Wu, Y., Li, P., & Chen, H. (2023). The characteristic and seasonal variation of mesoscale convective systems precipitation over North China. *Quarterly Journal of the Royal Meteorological Society*. https://doi.org/10.1002/qj.4510

Xie, S.-P., & Sampe, T. (2010). Large-scale dynamics of the Meiyu-Baiu rainband: Environmental forcing by the westerly jet. *Journal of Climate*, *23*(1), 113–134. https://doi.org/10.1175/2009jcli3128.1

Yang, Q., Houze, R. A., Jr., Leung, L. R., & Feng, Z. (2017). Environments of long-lived mesoscale convective systems over the central United States in convection permitting climate simulations. *Journal of Geophysical Research: Atmospheres*, *122*(24), 13–288. https://doi.org/10.1002/2017jd027033

Yang, R., Zhang, Y., Sun, J., Fu, S., & Li, J. (2019). The characteristics and classification of eastward-propagating mesoscale convective systems generated over the second-step terrain in the Yangtze River Valley. *Atmospheric Science Letters*, *20*(1), e874. https://doi.org/10.1002/asl.874

Zhang, Y., Zhang, F., Davis, C. A., & Sun, J. (2018). Diurnal evolution and structure of long-lived mesoscale convective vortices along the Mei-Yu front over the East China Plains. *Journal of the Atmospheric Sciences*, *75*(3), 1005–1025. https://doi.org/10.1175/jas-d-17-0197.1

References From the Supporting Information

Adler, R. F., Huffman, G. J., Chang, A., Ferraro, R., Xie, P. P., Janowiak, J., et al. (2003). The version-2 global precipitation climatology project (GPCP) monthly precipitation analysis (1979–present). *Journal of Hydrometeorology*, *4*(6), 1147–1167. https://doi.org/10.1175/1525-7541(2003)004<1147:tvgpcp>2.0.co;2

Joyce, R. J., Janowiak, J. E., Arkin, P. A., & Xie, P. (2004). CMORPH: A method that produces global precipitation estimates from passive microwave and infrared data at high spatial and temporal resolution. *Journal of Hydrometeorology*, *5*(3), 487–503. https://doi.org/10.1175/1525-7541(2004)005<0487:camtpg>2.0.co;2